JOURNAL OF APPLIED ELECTROCHEMISTRY 15 (1985) 475–484

*Growth kinetics of bubbles electrogenerated at microelectrodes**

N. P. BRANDON‡, G. H. KELSALL

Department of Mineral Resources Engineering, Imperial College, London SW7 2BP, UK

Received 12 November 1984

The growth kinetics of electrogenerated hydrogen, oxygen and chlorine gas bubbles formed at microelectrodes, were determined photographically and fitted by regression analysis to the equation; $r(t) = \beta t^x$, where $r(t)$ is the bubble radius at time t after nucleation, β the 'growth coefficient', and x the 'time coefficient'. The coefficient x was found to decrease from a short time (< 10 ms) value near unity, typical of inertia controlled growth, through 0.5, characteristic of diffusional control, to 0.3, expected for Faradaic growth, at long times (> 100 ms). The current efficiency for bubble growth increased with bubble lifetime, reflecting the decrease in local dissolved gas supersaturation. The pH dependency of the bubble departure diameter indicated that, in surfactant-free electrolytes, double layer interaction forces between the negatively charged hydrogen evolving cathode or positively charged oxygen/chlorine evolving anode and positively (pH < 2) or negatively (pH > 3) charged bubbles, were the determining factor. The effect of addition of an increasing concentration of cationic (DoTAB) or anionic (SDoS) surfactant was to progressively reduce the pH effect on departure diameter, due to surfactant adsorption on the bubble and, to a lesser extent, on the electrode.

Nomenclature

C	coefficient [3]
D	diffusion coefficient ($m^2 s^{-1}$)
I	current (μA)
P	pressure ($kN m^{-2}$)
R	universal gas constant (8.314 J $mol^{-1} K^{-1}$)
r	bubble radius (μm)
T	absolute temperature (K)
t	time (ms)
x	time coefficient
zF	molar charge (96 487z C mol^{-1})
β	growth coefficient ($m s^{-0.33}$)
ΔP	Laplace excess pressure ($kN m^{-2}$)
γ	surface tension ($mN m^{-1}$)
ρ	electrolyte density ($kg m^{-3}$)
θ	contact angle (°)

1. Introduction

An adequate description of the chemistry and physics involved in the nucleation, growth, detachment and coalescence of electrogenerated bubbles is of importance in the design of chlor-alkali cells, water electrolysers and electrowinning cells. Such information is also of value to those involved with the analogous process of nucleate boiling, and in electroflotation, for which control of the bubble size is important.

Westwater *et al.* [1, 2] observed that following an initial period of bubble growth dominated by liquid inertia and driven by the excess pressure ($r \alpha$ time), the kinetics followed Scriven's [3] theoretical description of diffusion-controlled spherical phase growth ($r \alpha \text{time}^{1/2}$). However, Verhaart *et al.* [4] found the bubble radius (r) to be proportional to $(\text{time})^{1/3}$ for a 100 μm diameter electrode, though Janssen [5] suggested that this applied only when the bubble was large compared to the electrode.

Most authors have found an increase in departure diameter with increasing current

*Paper presented at the International Meeting on Electrolytic Bubbles organized by the Electrochemical Technology Group of the Society of Chemical Industry, and held at Imperial College, London, 13–14 September 1984.

‡Present address: BP Research, Chertsey Road, Sunbury-on-Thames, Middlesex TW16 7LN, UK.

0021–891X/85 $03.00 + .12

density [6, 7], although pH has also been reported to have a significant effect. In alkaline solutions, cathodically evolved hydrogen bubbles had a smaller departure diameter than anodically evolved oxygen bubbles [8], whilst the converse was observed in acid solutions [9]. Organics such as alcohols have been found to decrease bubble surface areas/diameters [10, 11], which was ascribed to a decrease in surface tension.

The work reported here was an attempt to study the factors affecting bubble growth and departure diameters at micro-electrodes, such that the growth of single bubbles could be guaranteed under conditions of minimal surfactant contamination. Previous workers have paid little attention to electrolyte purity and have even unquestioningly reported the time dependency of bubble contact angles at supposedly hydrophilic electrodes [12, 13].

2. Experimental details

Details of the purification of the electrolytes used, the assessment of their purity and the construction of the electrochemical cell are given elsewhere [14, 15]. The electrodes were fabricated from 10 to 500 μm diameter 99.99% + platinum or silver wire (Goodfellow Metals plc) sealed into glass, using an applied vacuum for < 25 μm diameter wire to ensure a good glass-to-metal seal. The electrode and glass sleeve were then mounted in a syringe plunger, the barrel being part of the electrochemical cell, to enable adjustment of the position of the electrode surface in the cell. Mercury was used to make the connection with the electrode wire, and was encapsulated with epoxy resin. The electrode surface was then polished with a range of silicon carbide papers down to 10 μm grade, then with 0.3 μm alumina powder. The silver electrodes were also polished electrochemically using alkaline cyanide solutions [16]. The platinum electrode areas were determined by measurement of the hydrogen adsorption charge.

Potentiostatic or galvanostatic experiments were carried out using a Wenking MP81 potentiostat, a Hi-Tek Instruments waveform generator, a Nicolet Explorer 1 digital storage oscilloscope and a JJ Instruments *XY* recorder. Current and potential fluctuations were analysed using a Hewlett Packard HP5420A digital signal analyser and HP54470B digital filter. Impedance measurements were made using a Solartron 1250 frequency response analyser (FRA) and a Solartron 1186 Electrochemical Interface.

The bubble growth kinetics were determined using a horizontally mounted microscope coupled to a Link Electronics TV camera, Sony SL-F1UB video recorder and monitor. This system gave a time resolution of 20 ms and a magnification of up to 1000. For greater time resolution, a Hadlands Hyspeed camera (10–10 000 f.p.s.) with a light emitting diode timing generator was used.

Sodium sulphate, previously heated to red-heat to decompose organic contaminants, was used as supporting electrolyte at a concentration of 10 mol m^{-3} for hydrogen and oxygen bubble evolution, the pH being varied by sulphuric acid or sodium hydroxide additions. The same concentration of KCl was used as supporting electrolyte for chlorine bubble evolution, pH adjustment being made by additions of HCl or NaOH. All electrolytes were purged with gas generated at two platinum flag electrodes to remove any residual surfactant by ion flotation, the froth flowing out of the cell and over a weir. Electrolytes were then saturated from an external water electrolyser with the gas, the growth kinetics of which were to be studied. In later experiments, the cationic surfactant, dodecyltrimethylammonium bromide (DoTAB) or anionic surfactant, sodium dodecyl sulphate (SDoS) were deliberately added to the electrolytes to investigate their effects on bubble rise rates, Pt cyclic voltamograms, and bubble departure diameters.

3. Results and discussion

3.1. *Bubble growth kinetics*

Fig. 1 shows some typical hydrogen bubble diameter–time data at three current densities on a 25 μm Pt electrode. Very large current densities were needed to nucleate and grow bubbles as the rate of dissolved gas diffusion away from such small electrodes was high. An induction time for bubble nucleation was observed, being the time required to attain the necessary supersaturation of the electrolyte with respect to dissolved gas at the electrode surface. The degree of local supersaturation has been measured chronopotentio-

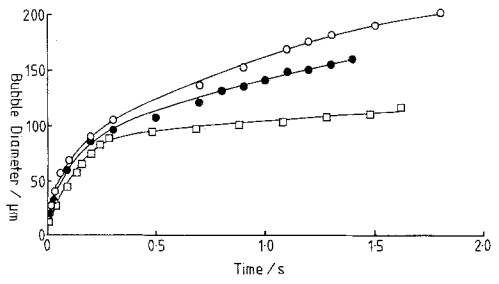

Fig. 1. Typical hydrogen bubble growth data for a 25 μm diameter Pt electrode at pH 1.4. □ 5 μA (10.2 kA m^{-2}), • 10 μA (20.4 kA m^{-2}), ○ 20 μA (40.8 kA m^{-2}).

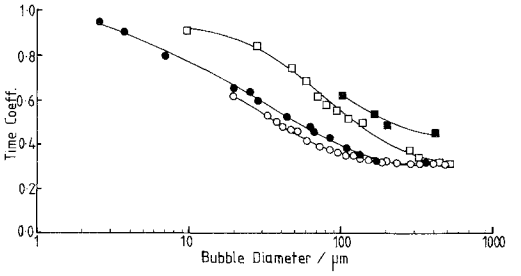

Fig. 3. Influence of bubble and electrode diameter on the time coefficient (x). ○ 10 μm, • 25 μm, □ 100 μm, ■ 500 μm diameter Pt.

metrically by Shibata for both hydrogen [17] and oxygen [18].

Following previous attempts [1, 4, 8] to define the bubble growth kinetics, the data were fitted by regression analysis to the equation

$$r(t) = \beta t^{x} \qquad (1)$$

where $r(t)$ is the bubble radius after t s of growth, β is the 'growth coefficient', principally dependent on the current density and independent of pH, and x is the 'time coefficient'. Fig. 2 shows x to be a time-dependent variable, being determined by the ratio of the bubble to electrode diameter (Fig. 3) and reflecting the different modes of bubble growth during its lifetime.

3.1.1. Growth coefficient (β). The growth coefficient (β) was dependent primarily on the current density and the faradaic charge per mole requirement of the gas generated, since at long times ($t >$ 100 ms)

$$r(t) = \beta t^{0.33} \qquad (2)$$

so that according to Faraday's and Charles' laws:

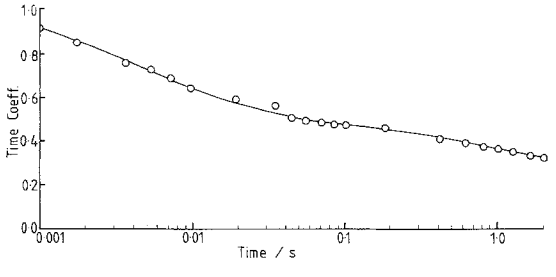

Fig. 2. Change in time coefficient (x) during hydrogen bubble growth on a 25 μm diameter Pt electrode at pH 1.4 and 10.2 kA m^{-2}.

$$\beta = \left(\frac{3RTI}{4\pi zFP}\right)^{0.33} \qquad (3)$$

The best fit of β vs $I^{0.33}$ was obtained at high current densities, corresponding to large bubble to electrode diameter ratios, where the 'direct injection' mode of growth would dominate over most of the lifetime of an individual bubble and the cumulative current efficiency would be high (Fig. 4). A current efficiency term could be included within Equation 3 to allow for the change in that parameter with time.

Solution pH had no effect on β for hydrogen or oxygen evolution, but for chlorine bubbles, the rate of growth decreased at high pH due to the formation of hypochlorite by the hydrolysis reaction

$$Cl_2 + 2\,OH^- = ClO^- + Cl^- + H_2O \qquad (4)$$

For the three gases studied, β decreased with rotation frequency for microelectrodes embedded in a glass rotating disc or cylinder, due to the dispersion of dissolved gas into the bulk electrolyte, so decreasing the current efficiency for bubble generation.

β had the same value under the same conditions for hydrogen generation at either platinum or silver electrodes, and no difference was found between mechanically and electrochemically polished silver electrodes. Addition of 10^{-5} to 1 mol m^{-3} sodium dodecyl sulphate or dodecyltrimethylammonium bromide had no effect on β, showing the growth rate to be independent of the mobility of the bubble interface [14, 15].

3.1.2. Time coefficient (x). At short times ($t <$ 10 ms), $x \to 1$ as bubbles grew by acting as sinks

for the previously generated dissolved gas, which formed a supersaturated solution adjacent to the electrode. Such growth is hydrodynamically controlled, being governed by liquid inertia, and may be described by the Rayleigh [19] equation:

$$r(t) = (2\,\Delta P/3\rho)^{0.5}\,t \qquad (5)$$

where ρ is the electrolyte density. In this period, bubble growth was driven by the high internal excess pressure (ΔP), which is related to the surface tension of the liquid–vapour interface (γ) by the Laplace equation for spherical bubbles:

$$\Delta P = 2\gamma/r \qquad (6)$$

The high initial growth rate resulted in a rapid decrease in the local supersaturation, such that diffusion of dissolved gas to the bubble surface became rate controlling. From $t = 10$ to 100 ms, the value of x was about 0.5 and the growth kinetics were described by an equation analogous to that derived by Scriven [3] for diffusion controlled spherical phase growth in an infinite, incompressible fluid:

$$r(t) = C(Dt)^{0.5} \qquad (7)$$

where C is a coefficient [3]. At long times (> 100 ms), when the bubble diameter exceeded that of the electrode, steep dissolved gas concentration gradients existed between the base of the bubble and the electrode, such that gas was injected almost directly into the bubble with little diffusional loss to the bulk solution, and $x \to 0.3$ (i.e. the bubble volume increased approximately linearly with time as expected from Faraday's law, allowing for some diffusional loss of dissolved gas to the bulk solution). This mode of growth became increasingly dominant as the ratio of bubble to electrode diameter increased.

Fig. 4 shows the effect of bubble diameter on the current efficiency (c.e.) for bubble production on electrodes of a range of diameters, where

$$\text{c.e.} = (zF/ItV_m)(4\pi r^3/3) \qquad (8)$$

with V_m representing the gas molar volume at the temperature of the experiment. The increase of the current efficiency with time/bubble diameter reflected the dominance of the direct injection growth mode at long times/large bubble diameters. 'Collection' of dissolved gas by the advancing bubble surface may also have been significant. The

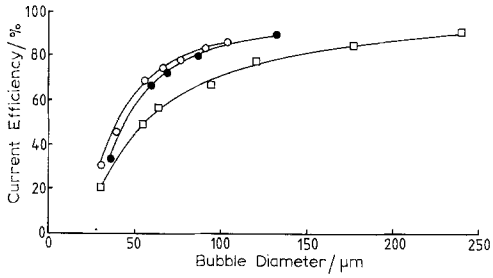

Fig. 4. Change in bubble current efficiency during bubble growth at ○ 10 μm, ● 25 μm, □ 100 μm diameter Pt electrodes at 20 μA.

greater the ratio of bubble to electrode diameter, the greater the current efficiency, since less dissolved molecular H_2, O_2 or Cl_2 diffused into the bulk solution. However, this would be sensitive to the local hydrodynamic regime.

Neither current density, electrode potential, electrode material/pretreatment, electrolyte, hydrodynamic conditions, or pH had any effect on the time coefficient, other than through their influence on the ratio of bubble to electrode diameter.

3.2. *Bubble departure diameters*

Figs. 5 and 6 show that the departure diameters of hydrogen bubbles were large at low pH and much smaller at high pH, the converse of the behaviour

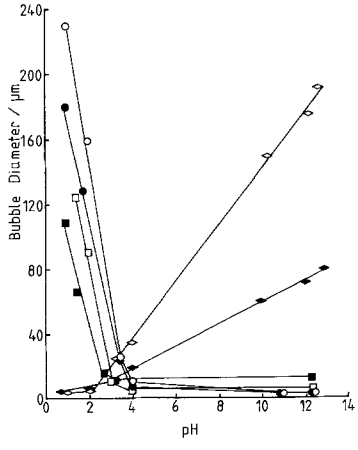

Fig. 5. Effect of pH on the departure diameter of H_2 (○ – 2.2 V, 10 μA; ● – 1.4 V, 5 μA; □ – 1.08 V, 1 μA; ■ – 0.78 V, 0.5 μA) and O_2 (◇ 3.2 V, 10 μA; ◆ 2.1 V, 1 μA) bubbles at a 10 μm diameter Pt electrode.

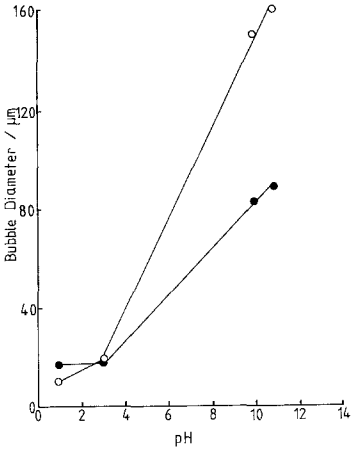

Fig. 6. Effect of pH on the departure diameter of Cl_2 bubbles at a 10 μm diameter Pt electrode. ○ 2.8 V, 5 μA; ● 2.2 V, 2 μA.

of oxygen and chlorine bubbles. These trends confirm earlier reports [8, 9], though the marked change in the slopes of the departure diameter–pH relationships and their crossing at pH 2–3 has not been reported previously.

The forces involved in holding a bubble at/on an electrode may arise from surface tension, if a contact angle (θ) is formed due to the presence of some hydrophobic (surfactant) species on the electrode surface. An analysis of the forces involved will be published later [20]. However, in the surfactant-free electrolytes used in this work, no measurable contact angle was observed, and the bubbles appeared to be tangent to the electrode surface, which therefore was assumed to be hydrophilic. At constant potential, the minimum in the current time series, just before bubble departure, was a significant fraction of the maximum current. This implies that any contact angle (θ) was extremely small or zero. For a 200 μm bubble (d_b) grown on a 10 μm diameter electrode (d_e), if $\theta > 2.8°$ then the condition $d_b \sin\theta > d_e$ would ensure the electrode–gas interface excluded any electrode–solution interface, and the current would be expected to fall to zero, which was never observed experimentally. The marked influence of pH on the bubble departure diameters, and the observation that bubbles departed from the electrode immediately when the current was interrupted or the modulus of the potential decreased sufficiently, support the view that forces other than surface tension were operative.

The bubbles have been shown [14, 15] to be charged even under surfactant-free conditions, with a point of zero charge at pH 2–3, i.e. they were negatively charged at pH > 3 and positively charged at pH < 2. It is proposed that electrostatic interaction between the bubble and electrode double layers controlled the bubble departure diameter, and that the two phases were separated by a thin liquid film of electrolyte. This hypothesis has been suggested previously [9], though without experimental evidence, but was rejected subsequently by Kabanov and Frumkin [12, 13]. However, their experimental work is not likely to have involved the surfactant-free electrolytes required to avoid surface tension forces dominating.

3.2.1. Electrode charge measurements. The charge on the electrode was determined from a.c. impedance measurements, which enabled the capacitance to be determined as a function of potential and pH, and hence the electrode charge (Fig. 7) to be calculated from the differential of the capacitance–potential relationship. The two minima in each plot in Fig. 7 correspond to the potentials of zero charge (p.z.c.) of platinum and at higher potentials, that of PtO_x. The effect of pH on these p.z.c.'s is shown in Fig. 8, the data for platinum being in reasonable agreement with those reported earlier [21]. The sharp increase in capacitance–differential charge at potentials in the hydrogen region was due to the adsorption pseudo-capacitance of hydrogen on the platinum, so precluding any definition of a p.z.c. for a hydride phase.

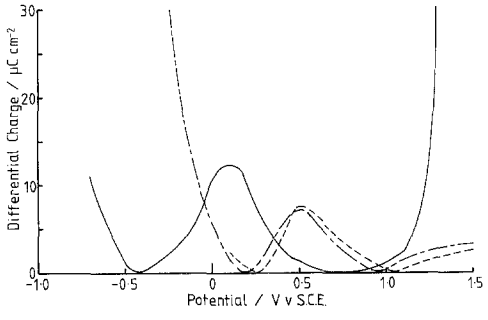

Fig. 7. Effect of potential and pH on the modulus of the differential charge of a Pt electrode (--- pH 1.3, —·— pH 1.9, —— pH 12).

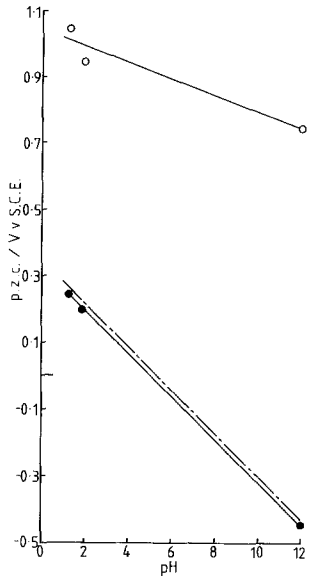

Fig. 8. Effect of pH on the potential of zero charge (p.z.c.) of Pt (•) and PtO_x (○). (-- data from [21]).

As the a.c. impedance technique does not discriminate experimentally between electrically and chemically stored charge, the former quantity is not defined in the hydrogen potential region, in the absence of a suitable model and data fitting procedure. Similarly, at high anodic potentials, the adsorption of oxygen causes the same confusion, so precluding any comparison of experimental bubble departure diameter data with theoretical predictions based on double layer interaction and buoyancy forces. The required information about the surface charge could be obtained either from fast galvanostatic/potentiostatic pulse experiments or by using microelectrophoresis of fine particles, the surface phase/potential of which could be controlled by suitable redox couples.

The effect of sodium dodecyl sulphate (SDoS) and dodecyltrimethylammonium bromide (DoTAB) surfactant additions on the differential charge as a function of potential, is given in Figs. 9 and 10, respectively. DoTAB decreased the p.z.c. by counteracting the negative charge on the electrode, whereas SDoS increased the p.z.c. by enhancing the negative electrode charge. Using a figure of 2.5×10^{-19} m^2 for the area occupied by an SDoS ion [22], the maximum fractional coverage of the electrode by SDoS was estimated as 0.24 and 0.37 at 0.7 V vs SHE. and pH 1.1 for 10^{-2} and 1 mol SDoS m^{-3}, respectively. Using a

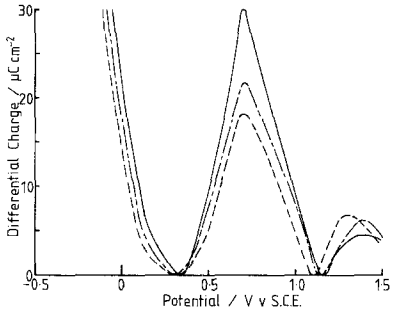

Fig. 9. Influence of SDoS concentration and potential on the modulus of the differential charge of a Pt electrode at pH 1.1, --- 10^{-4} mol SdoS m^{-3}, —— 10^{-2} mol SDoS m^{-3}, —— 1 mol SDoS m^{-3}.

cross sectional area of 2.6×10^{-19} m^2 for DoTAB [22], its maximum coverage was estimated as 0.11 at 0.6 V, pH 1.4 and 1 mol DoTAB m^{-3}. These low coverages may explain why only very small contact angles were observed for bubbles generated in the presence of these surfactants.

3.2.2. Effect of pH. At the potentials at which chlorine and oxygen would be evolved, say greater than 1.5 V vs SHE., the PtO_x surface would be positively charged, whereas for hydrogen evolution the electrode would be strongly negatively charged. An electrostatic interaction between such surfaces and bubbles which were negatively charged at pH > 3 and positively charged at pH < 2, would explain the results given in Figs. 5 and 6:

(a) The attraction between positively charged hydrogen bubbles and the negatively charged Pt

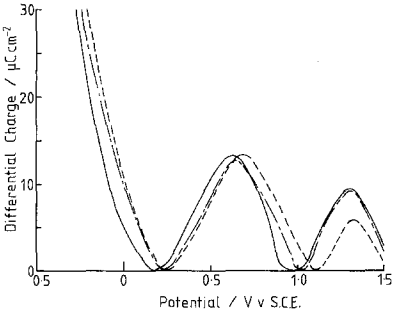

Fig. 10. Influence of DoTAB concentration and potential on the modulus of the differential charge of a Pt electrode at pH 1.4, --- 10^{-4} mol DoTAB m^{-3}, —— 10^{-2} mol DoTAB m^{-3}, —— 1 mol DoTAB m^{-3}.

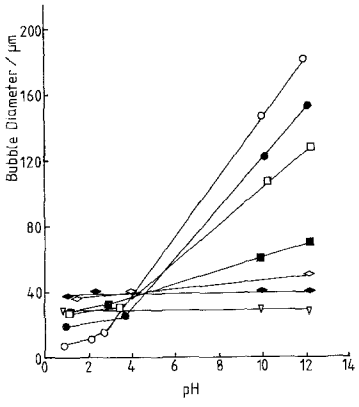

Fig. 11. Effect of DoTAB concentration and pH on the departure diameter of 0_2 bubbles from a 25 μm diameter Pt electrode at 40 kA m^{-2}. ○ surfactant-free, ● 10^{-5}, □ 10^{-3}, ■ 10^{-2}, ◇ 5×10^{-2}, ◆ 10^{-1}, ▽ 1 mol DoTAB m^{-3}.

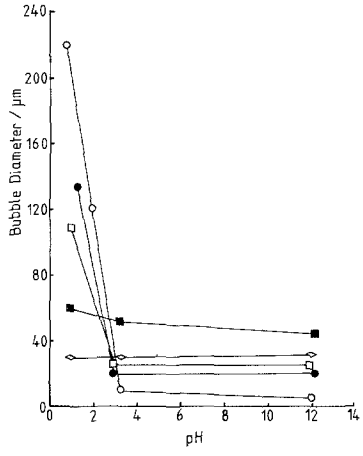

Fig. 12. Effect of DoTAB concentration and pH on the departure diameter of H_2 bubbles from a 25 μm diameter Pt electrode at 40 kA m^{-2}. ○ surfactant-free, ● 10^{-5}, □ 10^{-3}, ■ 10^{-1}, ◇ 1 mol DoTAB m^{-3}.

electrode, produced large diameters before buoyancy forces dominated, causing bubble departure. At higher pH the bubbles were negatively charged and electrostatic repulsion produced very small bubbles.

(b) Oxygen and chlorine bubbles were repelled from a positively charged PtO_x anode at pH < 2, and attracted at higher pH, such that the oxygen and chlorine bubble departure diameters increased with increasing pH, contrary to the behaviour of hydrogen bubbles.

Immediately after their nucleation, bubbles may have begun rising whilst appearing to grow at/on the electrode, due to the higher growth rates at shorter times, the very low rates of rise of such small bubbles [14, 15] and the consequently small distance risen in the time taken to reach the observed departure diameters.

3.2.3. Effect of surfactant addition. With DoTAB additions, the influence of pH on the departure diameter decreased with increasing DoTAB concentration for both oxygen (Fig. 11) and hydrogen (Fig. 12) bubbles. The adsorption of DoTAB at the gas–liquid interface produced an increasingly positive bubble electrophoretic mobility/charge with increasing concentration [14, 15]. DoTAB adsorption on the Pt electrode had already been established by impedance measurements (Fig. 10). The resulting decrease in the electrostatic attraction between bubble and electrode eventually masked the effect of pH and potential on the departure diameter, which was about 30 μm for both hydrogen and oxygen at a surfactant concentration of 1 mol m^{-3}. Addition of SDoS also reduced the departure diameter of both oxygen (Fig. 13) and hydrogen (Fig. 14) bubbles, for reasons similar to those proposed for the effect of DoTAB.

At pH values for which the sign of the charge on the bubbles was the same as that on the

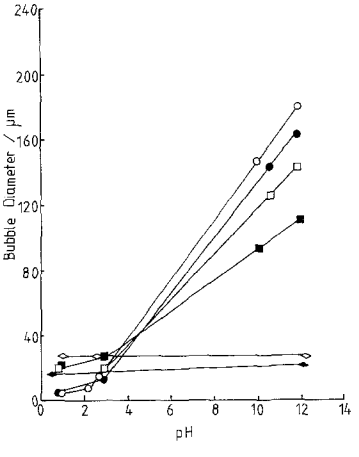

Fig. 13. Effect of SDoS concentration and pH on the departure diameter of 0_2 bubbles from a 25 μm diameter Pt electrode at 40 kA m^{-2}. ○ surfactant-free, ● 10^{-5}, □ 10^{-3}, ■ 10^{-2}, ◇ 10^{-1}, ◆ 1 mol SDoS m^{-3}.

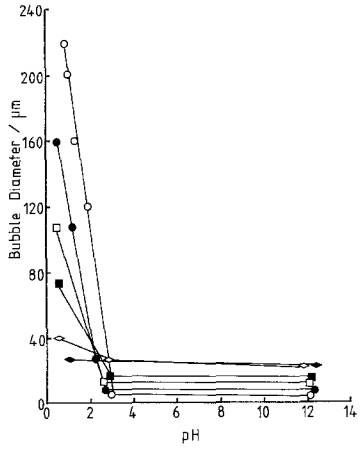

Fig. 14. Effect of SDoS concentration and pH on the departure diameter of H_2 bubbles from a 25 μm diameter Pt electrode at 40 kA m^{-2}. ○ surfactant-free, ● 10^{-5}, □ 10^{-3}, ■ 10^{-2}, ◇ 10^{-1}, ◆ 1 mol SDoS m^{-3}.

surfactant ions (pH $<$ 2 for DoTAB, pH $>$ 3 for SDoS), the dominant factor in reducing the bubble departure diameter (Figs. 12 and 13) was surfactant adsorption on the electrode. This resulted in a decrease in the electrode charge at low potentials with DoTAB and high potentials with SDoS, as shown in Figs. 9 and 10. Again, the overall effect was a decrease in the electrostatic interaction between the electrode and bubble, leading to a decrease in bubble departure diameter.

Very small bubbles ($<$ 10 μm diameter) remained on the electrode following current interruption at DoTAB concentrations greater than 10^{-1} mol m^{-3}, probably due to the presence of a very small contact angle ($< 1°$). This explained the increase in the lower limit of bubble departure diameter at such high concentrations.

Fig. 15 shows the practical benefit of a decrease in the electrode potential with increasing surfactant concentration, due to a decrease in the electrode–bubble electrostatic interaction and bubble departure diameter.

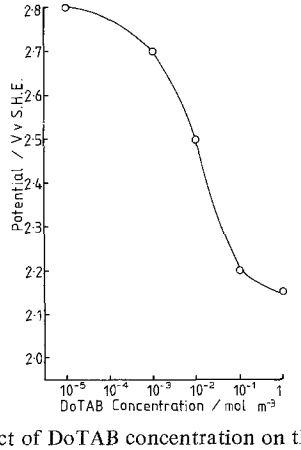

Fig. 15. Effect of DoTAB concentration on the apparent electrode potential for oxygen evolution at a 25 μm diameter Pt electrode at 20 kA m^{-2} and pH 12.3.

3.2.4. Effect of hydrodynamic regime. Fig. 16 shows the effect of rotation frequency on bubble departure diameter at a rotating disc electrode. As bubbles could not depart by buoyancy forces alone because of its downward facing geometry, large departure diameters were observed at low rotation frequencies, but with increasing radial flow at higher rotation rates, bubbles were swept from the electrode surface, probably also reflecting a degree of eccentricity in the rotation. To avoid the anomalous effect produced by the geometry of the downward-facing disc electrode, a microelectrode was embedded in the side of a rotating glass cylinder. The bubble departure diameter was much smaller than at a stationary upward-facing disc electrode, due to the shearing force generated by rotation and because most of the electrostatic attraction force was acting normal to the electrode surface and the buoyancy force.

Current efficiency for bubble generation at the Pt micro-disc electrode decreased with increasing

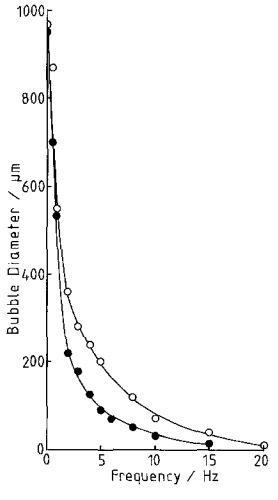

Fig. 16. Influence of rotation frequency on hydrogen bubble departure diameter from a 100 μm diameter Pt electrode embedded in glass, pH 1.2, ● 25.5 kA m^{-2}, ○ 63.5 kA m^{-2}.

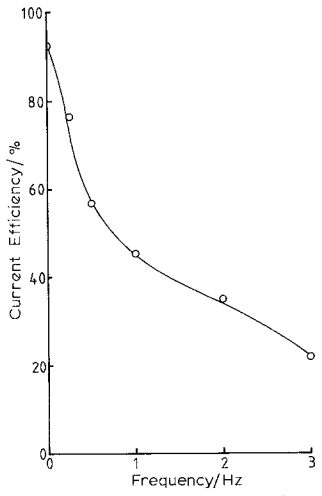

Fig. 17. Influence of rotation frequency on the current efficiency for hydrogen bubble generation at a 100 μm diameter rotating disc electrode, pH 1.2, 63.5 kA m^{-2}.

rotation frequency (Fig. 17), due to enhanced dissolved gas dispersion into the bulk electrolyte, in addition to the effect of the decrease in the ratio of bubble to electrode diameter (Fig. 4).

3.3. *Potential fluctuations due to bubble growth and departure*

The growth of bubbles at the microelectrodes caused distortion of the potential distribution, and hence the current density distribution, due to the dielectric gas phase obscuring the electrode. In addition, the local distribution of (supersaturated) dissolved hydrogen caused a decrease in the local equilibrium potential, according to the Nernst equation. The time dependence of the electrode potential was recorded by digital storage oscilloscope and/or analysed statistically in real time.

Fig. 18 shows a typical normalized amplitude probability density function for the electrode potential fluctuations at a 100 μm Pt electrode evolving hydrogen. The form of the function is as expected from the bubble growth kinetics, i.e. for an individual bubble, its initially high growth rate slowed with time, such that for most of its lifetime the electrode was largely obscured by the bubble. Hence the most probable potential was close to the maximum potential achieved. No correction was made for any ohmic potential loss in the quoted electrode potentials.

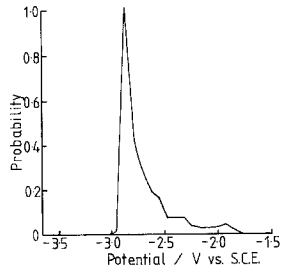

Fig. 18. Normalized amplitude probability density function for potential fluctuations at a 100 μm diameter Pt electrode evolving H_2 at 81 kA m^{-2}, pH 0.9.

The autocorrelation function of the same fluctuations was determined and Fourier transformed to give the power spectral density function shown in Fig. 19, in which the fundamental frequency at about 2.2 Hz corresponded to the observed bubble evolution rate. The other peaks in the spectrum were harmonics resulting from the form of the potential time series, reflecting the non-linearity of the electrode kinetics. By integration of the power spectra, the total power associated with the electrode potential fluctuations could be determined as a function of the diameter of the gas evolving electrode, as shown in Fig. 20. As expected, the power decayed rapidly with increasing electrode diameter, more so at higher current densities.

4. Conclusions

Three modes of growth of individual bubbles on microelectrodes have been observed during their lifetime: liquid inertia control, then diffusion control, followed by 'direct injection' when the bubble to electrode diameter ratio was large. The bubble departure diameter in surfactant-free electrolytes was found to be pH dependent, which

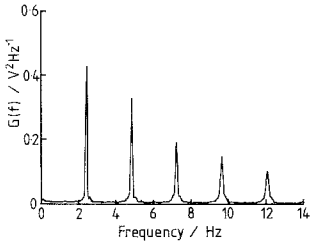

Fig. 19. Power spectral density function for conditions specified in Fig. 18, bubble departure diameter 260 μm.

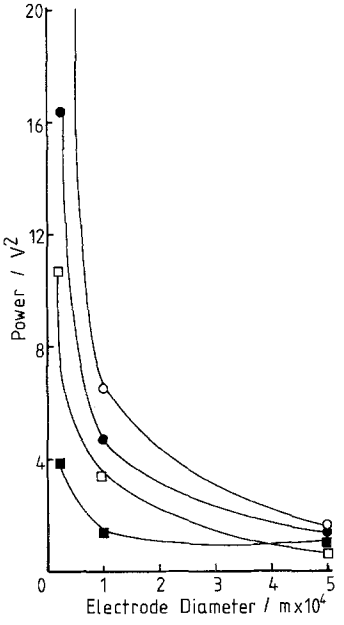

Fig. 20. Influence of electrode diameter on the power in the electrode potential fluctuations during hydrogen evolution at Pt electrodes at ■ 20, □ 40, ● 60, ○ 81 kA m^{-2}, pH 0.9.

in conjunction with other results [14, 15] showing a point of zero charge at pH 2–3, indicated that electrostatic interactions between double layer charges on the bubbles and electrode was the determining factor. A quantitative analysis of these interactions and of the forces involved when a contact angle is formed between the bubble and electrode in a surfactant-containing electrolyte, will be published later [20].

Acknowledgement

The authors thank the Science and Engineering Research Council (SERC) and Unilever Research plc for the provision of a CASE research studentship for NPB.

References

[1] J. P. Glas and J. W. Westwater, *Int. J. Heat Mass Transfer* 7 (1964) 1427.
[2] D. E. Westerheide and J. W. Westwater, *AIChE J.* 7 (1961) 351.
[3] L. E. Scriven, *Chem. Eng. Sci.* **1** (1959) 1.
[4] H. F. A. Verhaart, R. M. De Jonge and S. J. D. van Stralen, *Int. J. Heat Mass Transfer* **23** (1980) 293.
[5] L. J. J. Janssen, 'Boiling Phenomena', Vol. 1, (Edited by S. J. D. van Stralen and R. Cole) McGraw-Hill, New York (1979) Ch. 13.
[6] D. Landolt, R. Acosta, R. H. Muller and C. W. Tobias *J. Electrochem. Soc.* **117** (1970) 839.
[7] R. M. De Jonge, E. Barendrecht, L. J. J. Janssen and S. J. D. van Stralen, Proceedings of the 3rd World Hydrogen Conference, Tokyo (1980), pp. 195–207.
[8] C. W. Sillen, E. Barendrecht, L. J. J. Janssen and S. J. D. van Stralen, *ibid* pp. 175–193.
[9] A. Coehn and H. Neumann, *Z. Phys.* **20** (1923) 54.
[10] M. J. Blandamer, F. Franks, K. H. Haywood and A. C. Tory, *Nature* **216** (1967) 783.
[11] J. Venczel, *Electrochim. Acta* **15** (1970) 1909.
[12] B. Kabanov and A. N. Frumkin, *Z. Phys. Chem.* **165** (1933) 433.
[13] *Idem*, *ibid.* **166** (1934) 316.
[14] N. P. Brandon, G. H. Kelsall, S. Levine and A. L. Smith, *J. Appl. Electrochem.* **15** (1985) 485.
[15] N. P. Brandon, Ph.D. Thesis, University of London, (1985).
[16] W. J. McG.Tegart, 'The Electrolytic and Chemical Polishing of Metals', Pergamon, London (1956).
[17] S. Shibata, *Bull. Chem. Soc. Jpn* **36** (1963) 53.
[18] S. Shibata, *Electrochim. Acta* **23** (1978) 619.
[19] Lord Rayleigh, *Philos. Mag.* **94** (1917).
[20] N. P. Brandon and G. H. Kelsall, to be published.
[21] E. Gileadi, S. D. Argade and J. O'M.Bockris, *J. Phys. Chem.* **70** (1966) 2044.
[22] J. Rogers, *Trans IMM* **66** (1957) C439.
[23] S. K. Doss, *ibid.* 85 (1976) C195.